

Neural ODE and DAE Modules for Power System Dynamic Modeling

Tannan Xiao, Ying Chen, Tirui He, and Huizhe Guan

Abstract—The time-domain simulation is the fundamental tool for power system transient stability analysis. Accurate and reliable simulations rely on accurate dynamic component modeling. In practical power systems, dynamic component modeling has long faced the challenges of model determination and model calibration, especially with the rapid development of renewable generation and power electronics. In this paper, based on the general framework of neural ordinary differential equations (ODEs), a modified neural ODE module and a neural differential-algebraic equations (DAEs) module for power system dynamic component modeling are proposed. The modules adopt an autoencoder to raise the dimension of state variables, model the components' dynamics with artificial neural networks (ANNs), and keep the numerical integration structure. In the neural DAE module, an additional ANN is used to calculate injection currents. The neural models can be easily integrated into time-domain simulations. With datasets consisting of sampled curves of input variables and output variables, the proposed modules can be used to fulfill the tasks of parameter inference, physics-data-integrated modeling, black-box modeling, etc., and can be easily integrated into power system dynamic simulations. Some simple numerical tests are carried out in the IEEE-39 system and prove the validity and potentiality of the proposed modules.

Index Terms—Power system dynamics, power system simulations, dynamic modeling, differential equations, differential-algebraic equations, neural networks, autoencoder

I. INTRODUCTION

FROM the perspective of power systems, ensuring the normal and healthy functioning of components and the stable operation of the system is a crucial task. The success of this task relies heavily on accurate dynamic component modeling and power system dynamic simulations [1].

Power system dynamic component modeling is already a mature and generally researched area [2]. For the equipment whose physics is clear, the model can be easily determined or selected. The difficulty of obtaining an accurate model lies in model calibration, which is essentially a parameter inference or estimation problem. For the equipment whose physics is still under research or the equivalent load modeling problem, both the model and parameters need determination. Simulations based on inaccurately modeled power systems cannot

accurately predict the system state and may even lead to completely wrong stability judgment. For the topic of power system stability analysis, model determination and model calibration are the two crucial problems, especially with the rapid development of renewable generation and power electronics. This is the reason why these topics are well studied and researchers are still pursuing the studies on these topics.

As for the model determination problem, intuitively, dynamic components such as generating units, loads, regulators, etc., can be modeled based on their physics. It is the traditional and inevitable way of obtaining an accurate dynamic model that can be used in power system simulations. There have been continuing studies down this path and many physics-based models have been proposed, e.g., 2nd-order to 6th-order generator models [3], induction motor model [3], generic models for wind turbines [4], the single diode solar cell model [5], the battery energy storage system model in the d-q axes [6], the average-value model of high-speed response brushless excitation systems [7], the IEEE1 governor model [8], the multi-band power system stabilizer [9], etc. On the other hand, from the point of view of transmission networks, feeders in the substations, networked microgrids, traditional distribution networks, and active distribution networks containing distributed generations will usually be modeled as equivalent dynamic load models. A comprehensive review of load modeling can be found in [10]. The load model is usually selected by the operators based on their experience and the dynamic characteristics of the components in the network. Therefore, the load modeling of practical power systems often shows regional characteristics [2].

As for the model calibration problem, the most traditional way is to directly calculate the parameters by obtaining needed measurements in field tests that are designed based on physics. Various measurement-based model calibration methods, which are essentially a posterior optimization approach, have been proposed. A weighted least-square estimation algorithm that obtains the maximum likelihood estimation of the parameters is presented in [11]. Optimization-based methods formulate the parameter estimation problem as an optimization problem and solve it using gradient-based algorithms [12], trajectory sensitivity-based algorithms [13], and meta-heuristic algorithms [14]. Kalman filter-based methods calibrate the parameters by representing the probability density function of the augmented state variables [15], [16]. Bayesian inference-based algorithms optimize the parameters by minimizing the errors of approximate posteriors [17], [18].

Research on machine learning (ML) has achieved a growth

This paper is first submitted to IEEE. This work was supported in part by the National Natural Science Foundation of China (NSFC) under the Project No. 52107104, (Corresponding Author: Ying Chen).

All the authors are with the Department of Electrical Engineering, Tsinghua University, Beijing, 100084, China (Email: ceexiaoxh@gmail.com, hetirui@qq.com, mark.mghz@gmail.com, chen_ying@tsinghua.edu.cn).

spurt in the past few years. ML algorithms have been applied to a variety of power system studies including dynamic component modeling. Reinforcement learning algorithms [19] calibrate model parameters by establishing an agent-environment interactive mechanism. Deep learning algorithms are directly used for model calibration [20] or to identify Koopman eigenfunctions for linear representation of nonlinear systems [21]. Neural ordinary differential equations (ODEs) proposed in [22] have been used to establish neural models for networked microgrids for reachability analysis [23]. The framework of neural ODE has drawn a lot of attention. Compared with other methods, neural ODEs keep the numerical integration structure, which is a very important prior knowledge. The framework has inspired many data-physics-integrated studies such as neural partial differential equations [24], the Hamilton neural networks [25], and the Lagrangian neural networks [26]. These studies have demonstrated the great potential of neural ODE in solving the dynamics of physical systems.

In practical power systems, dynamic component modeling has long faced the challenges of model determination and model calibration, especially with the rapid development of renewable generation and power electronics. On the one hand, some new devices' physics are still under research. We may not have enough prior knowledge to construct or select a proper model. The measurable variables might also be limited, which means only partial dynamics is observable. On the other hand, some new devices' dynamic models are completely black-boxes due to the confidential protocols of the equipment companies. The only accessible knowledge is the input and output settings of the equipment. Although a dynamic link library (DLL) file for dynamic simulations is usually available, the DLL file can seriously degrade the efficiency of the simulation program and affect the gradient calculation process for stability control. In these situations, model determination and model calibration should be done at the same time with only very limited or even no prior knowledge except the input and output settings. The constructed model should be easy to integrate into dynamic simulations and keep the accuracy and efficiency of simulations. Within the aforementioned methods, the neural ODE-based approach seems a promising way to fill this gap.

In this paper, we explore the application of neural ODE [22] in power system dynamic component modeling and transient stability simulations. Based on the general framework of neural ODE, we design and implement a modified neural ODE module and a neural differential-algebraic equations (DAE) module for power system dynamic component modeling. An autoencoder is used to improve the performance of the proposed modules. Tests are carried out in the IEEE-39 system under the scenarios of parameter estimation, physics-data-integrated component modeling, and black-box modeling. The obtained models are integrated into a simulation program and simulation results are compared with the original models.

The remainder of the papers is as follows. Section II provides the theoretical background of power system simulations and the original neural ODE. The proposed modules are illustrated in

Section III and numerical tests are carried out in Section IV. Discussions of the proposed modules and the neural ODE-based modeling method are shown in Section V. Conclusions are drawn in Section VI.

II. THEORETICAL BACKGROUND

This section will give a brief mathematical introduction to power system dynamic simulations and neural ODE.

A. Power System Dynamic Simulations

The overall system DAEs, including differential equations (DEs) (1) for all the dynamic devices and algebraic equations (AEs) (2) for the network, need to be solved during the power system transient stability simulation:

$$\dot{\mathbf{x}} = \mathbf{f}(\mathbf{x}, \mathbf{V}) \quad (1)$$

$$\mathbf{G}(\mathbf{x}, \mathbf{V}) = \mathbf{Y}\mathbf{V} - \mathbf{I}(\mathbf{x}, \mathbf{V}) = \mathbf{0} \quad (2)$$

where \mathbf{x} is the state vector of the system, whose time derivatives are equal to $\mathbf{f}(\mathbf{x}, \mathbf{V})$, \mathbf{V} is the bus voltage vector, \mathbf{I} is the injection current vector, \mathbf{Y} is the admittance matrix.

Power system dynamic component modeling constructs the mathematical models of the components with DEs and AEs so that the models can be integrated into DAEs. The dynamic components in the power system can be divided into two types according to whether the component produces injection currents into the power network.

These equations can be solved by the simultaneous approach or by the alternating approach. In the simultaneous approach, after applying implicit numerical integration methods to DEs, DEs will transform into algebraic equations and can be solved simultaneously with (2) using the Newton method iteratively, as shown in (3)-(4):

$$\begin{bmatrix} \mathbf{F}(\mathbf{x}, \mathbf{V}) \\ \mathbf{G}(\mathbf{x}, \mathbf{V}) \end{bmatrix} = \begin{bmatrix} \mathbf{0} \\ \mathbf{0} \end{bmatrix} \quad (3)$$

$$\begin{bmatrix} \frac{\partial \mathbf{F}}{\partial \mathbf{x}} & \frac{\partial \mathbf{F}}{\partial \mathbf{V}} \\ \frac{\partial \mathbf{G}}{\partial \mathbf{x}} & \frac{\partial \mathbf{G}}{\partial \mathbf{V}} \end{bmatrix} \begin{bmatrix} \Delta \mathbf{x} \\ \Delta \mathbf{V} \end{bmatrix} = \begin{bmatrix} -\mathbf{F} \\ -\mathbf{G} \end{bmatrix} \quad (4)$$

where $\mathbf{F}(\mathbf{x}, \mathbf{V})$ are the algebraic equations obtained by applying numerical integration methods to DEs.

On the other hand, in the alternating approach, the DEs and AEs are solved separately. First, given the state vector $\mathbf{x}(t)$ and bus voltage vector $\mathbf{V}(t)$ at instant t , estimate the initial value $\mathbf{V}^{(0)}(t + \Delta t)$, or simply let $\mathbf{V}^{(0)}(t + \Delta t) = \mathbf{V}(t)$. Second, solve (1) to obtain $\mathbf{x}^{(0)}(t + \Delta t)$ using the numerical integration method with $\mathbf{x} = \mathbf{x}(t)$ and $\mathbf{V} = \mathbf{V}^{(0)}(t + \Delta t)$. Third, solve (2) for $\mathbf{V}^{(1)}(t + \Delta t)$ with $\mathbf{x} = \mathbf{x}^{(0)}(t + \Delta t)$ and $\mathbf{V} = \mathbf{V}^{(0)}(t + \Delta t)$. Then solve (1) again with $\mathbf{x} = \mathbf{x}^{(0)}(t + \Delta t)$ and $\mathbf{V} = \mathbf{V}^{(1)}(t + \Delta t)$. The above iteration is repeated until convergence is reached. Fast solution techniques [27] can be used to improve numerical stability and accelerate the solution processes.

As can be seen, the simultaneous approach is more strict and the dynamic component models must support the calculation of partial derivatives shown in (4). The DLL files provided by the equipment company cannot provide derivative information in most of the cases, i.e., they cannot be solved using the

simultaneous approach. In contrast, the alternating approach will cause errors and affect the simulation accuracy, but this approach is still widely used in industry-grade simulation programs because of its programming flexibility and simplicity, reliability, and robustness [3]. Any dynamic model can be easily solved using this approach, including a DLL-based black-box model.

B. Neural ODE

The structure of the original Neural ODE module, as shown in Fig. 1(a), was first proposed by Chen *et al* in 2018 [22]. A neural ODE block consisting of neural networks is used to formulate a parameterized derivative function for derivative regression, as shown in (5):

$$\mathbf{f}_\theta(\mathbf{x};\theta) \doteq \dot{\mathbf{x}} = \mathbf{f}(\mathbf{x}) \quad (5)$$

where θ denotes parameters of the neural ODE block. Given the initial values $\mathbf{x}(0)$, the integration step Δt , and the integration time T , a series of \mathbf{x} can be easily calculated using a numerical integration method and the derivative function (5). For the convenience of demonstration, all the modules displayed in Fig. 1 use the Euler method.

The neural ODE block can be trained with a training set containing sample curves of \mathbf{x} . In (6), a loss function \mathcal{L} is defined to optimize θ :

$$\begin{aligned} \theta &= \arg \min_{\theta} \sum_{i=1}^N \mathcal{L}(\mathbf{x}_i, \hat{\mathbf{x}}_i; \theta) \\ \text{s.t. } \dot{\mathbf{x}}_i &= \mathbf{f}_\theta(\mathbf{x}_i; \theta), \mathbf{x}_i(0) = \hat{\mathbf{x}}_i(0), t \in [0, T] \\ \dot{\hat{\mathbf{x}}}_i &= \mathbf{f}(\hat{\mathbf{x}}_i), \hat{\mathbf{x}}_i(0) = \hat{\mathbf{x}}_i(0), t \in [0, T] \end{aligned} \quad (6)$$

where N denotes the number of samples in the training set, \mathbf{x} denotes the series of state variables predicted using the neural ODE module, and $\hat{\mathbf{x}}$ denotes the ground-truth series of state variables.

As can be seen, with the same input $\hat{\mathbf{x}}_i(0)$, a predicted curve \mathbf{x}_i and a ground-truth curve $\hat{\mathbf{x}}_i$ can be obtained.

To optimize θ , the widely used adjoint sensitivity method [28], which is also introduced in [22] and [23], can be adopted. By forming a Hamiltonian \mathcal{H} [29], as shown in (7), the gradients with respect to θ can be calculated with a backward integration as shown in (8):

$$\mathcal{H}(\mathbf{x}; \theta, \lambda) = \lambda^T \mathbf{f}_\theta(\mathbf{x}; \theta) \quad (7)$$

$$\nabla_{\theta} \mathcal{L} = \frac{\partial \mathcal{L}}{\partial \theta} = \int_r^0 \frac{\partial \mathcal{H}}{\partial \theta} dt = \int_r^0 \lambda^T \frac{\partial \mathbf{f}_\theta}{\partial \theta} dt \quad (8)$$

where λ denotes the Lagrange multiplier, the time derivatives of λ obey (9), and $\lambda(T)$ obeys (10):

$$\dot{\lambda} = -\frac{\partial \mathcal{H}}{\partial \mathbf{x}} = -\lambda^T \frac{\partial \mathbf{f}_\theta}{\partial \mathbf{x}} \quad (9)$$

$$\lambda(T) = \frac{\partial \mathcal{L}}{\partial \mathbf{x}(T)} \quad (10)$$

Like the forward integration, a numerical integration method can be used to solve the backward integration using a negative integration step $-\Delta t$. The parameters can be easily optimized after the gradients $\nabla_{\theta} \mathcal{L}$ are obtained, e.g., by applying the stochastic gradient descent method or the Adam optimizer [30].

The PyTorch[31]-based package of the original neural ODE

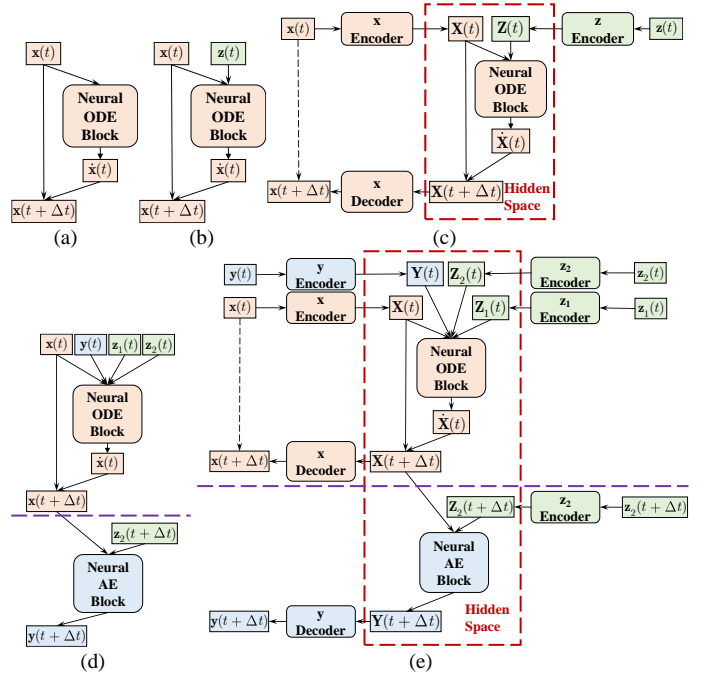


Fig. 1. Structures of (a) original neural ODE module, (b) modified neural ODE module, (c) autoencoder-based modified neural ODE module, (d) neural DAE module, and (e) autoencoder-based neural DAE module.

module can be found on GitHub [22]. Better implementations of neural ODE with lower memory cost have been improved in [32] and [33]. In these references, the loss function focuses more on the precision of the endpoint $\mathbf{x}(T)$.

III. MODIFIED NEURAL ODE MODULE AND NEURAL DAE MODULE

Based on the original neural ODE module shown in Fig. 1(a), we propose new designs of a modified neural ODE module in Fig. 1(b) and a neural DAE module in Fig. 1(d) for power system transient stability simulations.

A. Modified Neural ODE Module

In power system transient stability simulations, the dynamic components can be divided into two types according to whether the component produces injection currents into the power network. For the ones that do not produce injection currents into the power network, the dynamics of the component and the neural derivative function can be formulated as (11):

$$\mathbf{f}_\theta(\mathbf{x}, \mathbf{z}; \theta) \doteq \dot{\mathbf{x}} = \mathbf{f}(\mathbf{x}, \mathbf{z}) \quad (11)$$

where \mathbf{z} denotes the necessary input variables besides state variables \mathbf{x} . Accordingly, a modified neural ODE module is shown in Fig. 1(b). Taking an exciter as an example, in addition to the state variables, the nodal voltage of the generator-connected bus is also needed for calculating derivatives, i.e., the nodal voltage $V \in \mathbf{z}$. Meanwhile, the initial values of the state variables may be needed to determine the reference variables, e.g., the reference voltage of an exciter is calculated according to the steady-state value, i.e., power flow results. Therefore, the initial values of state variables $\mathbf{x}(0)$ might belong to \mathbf{z} . The equality constraint (12) is added to (6):

$$\mathbf{z}_i = \hat{\mathbf{z}}_i, t \in [0, T] \quad (12)$$

where $\hat{\mathbf{z}}$ denotes the ground-truth values of \mathbf{z} . After applying

the adjoint sensitivity method, the gradients can be calculated as in (7)-(10) by changing $\mathbf{f}_\theta(\mathbf{x};\theta)$ to $\mathbf{f}_\theta(\mathbf{x},\mathbf{z};\theta)$ and parameters θ can be optimized.

B. Neural DAE Module

For the components that produce injection currents into the power network, a more complex module illustrated in Fig. 1. (d) is designed by adding a neural AE block. The dynamics can be modeled using DAEs and be approximated using the neural DAE module as follows:

$$\mathbf{f}_\theta(\mathbf{x}, \mathbf{z}_1, \mathbf{y}, \mathbf{z}_2; \theta) \doteq \dot{\mathbf{x}} = \mathbf{f}(\mathbf{x}, \mathbf{z}_1, \mathbf{y}, \mathbf{z}_2) \quad (13)$$

$$\begin{aligned} \mathbf{G}_\xi(\mathbf{x}, \mathbf{y}, \mathbf{z}_2; \xi) &= \mathbf{y} - \mathbf{g}_\xi(\mathbf{x}, \mathbf{z}_2; \xi) \doteq \mathbf{0} \\ &= \mathbf{G}(\mathbf{x}, \mathbf{y}, \mathbf{z}_2) = \mathbf{y} - \mathbf{g}(\mathbf{x}, \mathbf{z}_2) \end{aligned} \quad (14)$$

where \mathbf{g} is the original functions of calculating \mathbf{y} with \mathbf{x} and \mathbf{z}_2 , \mathbf{G}_ξ denotes the neural AEs, \mathbf{g}_ξ denotes the neural AE block, ξ is the parameters of the neural AE block, \mathbf{y} denotes the output of AEs such as the injection currents, \mathbf{z}_2 is the input variables needed to calculate \mathbf{y} besides \mathbf{x} such as the nodal voltages, and \mathbf{z}_1 denotes the input variables needed to calculate $\dot{\mathbf{x}}$ besides \mathbf{x} , \mathbf{z}_1 , and \mathbf{y} . Taking a generator as an example, the inner electric potentials, rotor angle, rotor speed, and state variables of regulators belong to \mathbf{x} , the active power and reactive power belongs to \mathbf{z}_1 , the injection current belongs to \mathbf{y} , and the nodal voltage belongs to \mathbf{z}_2 . In many cases, \mathbf{g} is $\mathbf{I}(\mathbf{x}, \mathbf{V})$ in (2).

Similarly, a loss function can be defined for the optimization of θ and ξ , as shown in (15):

$$\begin{aligned} \theta, \xi &= \arg \min_{\theta, \xi} \sum_{i=1}^N \mathcal{L}(\mathbf{x}_i, \hat{\mathbf{x}}_i, \mathbf{y}_i, \hat{\mathbf{y}}_i; \theta, \xi) \\ \text{s.t.} \quad &\begin{cases} \dot{\mathbf{x}}_i = \mathbf{f}_\theta(\mathbf{x}_i, \mathbf{z}_{1i}, \mathbf{y}_i, \mathbf{z}_{2i}; \theta) \\ \mathbf{G}_\xi(\mathbf{x}_i, \mathbf{y}_i, \mathbf{z}_2; \xi) = \mathbf{y} - \mathbf{g}_\xi(\mathbf{x}_i, \mathbf{z}_2; \xi) = \mathbf{0} \\ \mathbf{x}_i(0) = \hat{\mathbf{x}}_i(0), \mathbf{y}_i(0) = \hat{\mathbf{y}}_i(0), t \in [0, T] \\ \begin{cases} \dot{\hat{\mathbf{x}}}_i = \mathbf{f}(\hat{\mathbf{x}}_i, \hat{\mathbf{z}}_{1i}, \hat{\mathbf{y}}_i, \hat{\mathbf{z}}_{2i}) \\ \mathbf{G}(\hat{\mathbf{x}}_i, \hat{\mathbf{y}}_i, \hat{\mathbf{z}}_{2i}) = \hat{\mathbf{y}}_i - \mathbf{g}(\hat{\mathbf{x}}_i, \hat{\mathbf{z}}_{2i}) = \mathbf{0} \end{cases} \\ \hat{\mathbf{x}}_i(0) = \hat{\mathbf{x}}_i(0), \hat{\mathbf{y}}_i(0) = \hat{\mathbf{y}}_i(0), t \in [0, T] \\ \mathbf{z}_{1i} = \hat{\mathbf{z}}_{1i}, t \in [0, T] \\ \mathbf{z}_{2i} = \hat{\mathbf{z}}_{2i}, t \in [0, T] \end{cases} \end{aligned} \quad (15)$$

where $\hat{\mathbf{y}}$, $\hat{\mathbf{z}}_1$, and $\hat{\mathbf{z}}_2$ denote the ground-truth values of \mathbf{y} , \mathbf{z}_1 , and \mathbf{z}_2 , respectively. The adjoint sensitivity method can also be used to derive gradients with respect to θ and ξ , which has the same form as the trajectory sensitivity method in the research field of power systems. The Hamiltonian \mathcal{H} is defined in (16) and the gradients can be calculated as shown in (17) and (18).

$$\mathcal{H}(\mathbf{x}, \mathbf{z}_1, \mathbf{y}, \mathbf{z}_2; \theta, \xi, \lambda, \beta) = \lambda^T \mathbf{f}_\theta(\mathbf{x}, \mathbf{z}_1, \mathbf{y}, \mathbf{z}_2; \theta) + \beta^T \mathbf{G}_\xi(\mathbf{x}, \mathbf{y}, \mathbf{z}_2; \xi) \quad (16)$$

$$\begin{aligned} \nabla_\theta \mathcal{L} &= \frac{\partial \mathcal{L}}{\partial \theta} = \int_T^0 \frac{\partial \mathcal{H}}{\partial \theta} dt = \int_T^0 \lambda^T \frac{\partial \mathbf{f}_\theta}{\partial \theta} + \beta^T \frac{\partial \mathbf{G}_\xi}{\partial \theta} dt \\ &= \int_T^0 \lambda^T \frac{\partial \mathbf{f}_\theta}{\partial \theta} + \beta^T \frac{\partial \mathbf{x}}{\partial \theta} \frac{\partial \mathbf{G}_\xi}{\partial \mathbf{x}} dt \end{aligned} \quad (17)$$

$$\nabla_\theta \mathcal{L} = \frac{\partial \mathcal{L}}{\partial \xi} = \int_T^0 \frac{\partial \mathcal{H}}{\partial \xi} dt = \int_T^0 \beta^T \frac{\partial \mathbf{G}_\xi}{\partial \xi} dt \quad (18)$$

where λ and β denotes the Lagrange multipliers, β and the time derivatives of λ obey (19) and (20), and $\lambda(T)$ obeys (21):

$$\dot{\lambda} = -\frac{\partial \mathcal{H}}{\partial \mathbf{x}} = -\lambda^T \frac{\partial \mathbf{f}_\theta}{\partial \mathbf{x}} - \beta^T \frac{\partial \mathbf{G}_\xi}{\partial \mathbf{x}} \quad (19)$$

$$\mathbf{0} = \frac{\partial \mathcal{H}}{\partial \mathbf{y}} = \lambda^T \frac{\partial \mathbf{f}_\theta}{\partial \mathbf{y}} + \beta^T \frac{\partial \mathbf{G}_\xi}{\partial \mathbf{y}} \quad (20)$$

$$\lambda(T) = \frac{\partial \mathcal{L}}{\partial \mathbf{x}(T)} \quad (21)$$

Similarly, we can derive gradients with respect to θ and ξ using a backward numerical integration.

C. Loss Function and Training Procedures

The previous two subsections illustrate how to derive gradients for the modified neural ODE module and the neural DAE module. For the convenience of demonstration, we take (\mathbf{x}, \mathbf{z}) and the modified neural ODE module as the example hereafter.

As for the loss function, the L1 norm (22) or the L2 norm (23) of the differences between the predicted curves and the ground-truth curves can be adopted.

$$\mathcal{L} = \mathbf{w}^T \|\mathbf{x} - \hat{\mathbf{x}}\| \quad (22)$$

$$\mathcal{L} = \mathbf{w}^T \|\mathbf{x} - \hat{\mathbf{x}}\|_2 \quad (23)$$

where \mathbf{w} denotes the weighting factors of different state variables. As mentioned before, the stochastic gradient descent method or the Adam optimizer can be applied to train the neural modules. The training procedures are as follows.

Training Procedures of Neural Modules

Input the total number of samples N , the integration step Δt , the simulation time T , the mini-batch size m , the number of training epochs E , evaluation interval ΔE ;

Get sample curves of $(\hat{\mathbf{x}}, \hat{\mathbf{z}})$ by simulations with simulation time T and fixed integration step Δt . Split the samples to form a training dataset and a testing dataset.

for $i=1$ **to** E **do**

for $j=1$ **to** N/m **do**

 Sample a mini-batch of m samples $(\hat{\mathbf{x}}, \hat{\mathbf{z}})$ from the training dataset

 Input $(\hat{\mathbf{x}}(0), \hat{\mathbf{z}})$ into the neural module and get \mathbf{x}

 Update $\theta \leftarrow \min_\theta \mathcal{L}(\mathbf{x}, \hat{\mathbf{x}}; \theta)$

end for

if $i \bmod \Delta E$ **then**

 Evaluate the neural module in the testing dataset

end if

end for

It should be noted that, strictly speaking, \mathbf{z} should be refreshed as the predicted \mathbf{x} changes, i.e., \mathbf{x} and \mathbf{z} should be predicted by solving the modified neural ODE module-integrated power system DAEs, instead of directly using the ground-truth value as in (12). However, the gradients will become much more difficult to calculate. The tests illustrated in [23] and in this paper all prove that training the neural module by directly using the ground-truth \mathbf{z}_j can achieve accurately

enough models and the implementation is much easier.

D. Event Handling

During simulations, events such as faults and relay actions will introduce jump changes to the network and operation variables such as nodal voltages and injection currents. Taking Fig. 1. (b) as an example, the state variable $\mathbf{x}(t)$ will not change right before and after the event, i.e., $\mathbf{x}(t^+) = \mathbf{x}(t^-)$, whereas some variables in $\mathbf{z}_1(t)$ may change, i.e., $\mathbf{z}_1(t^+) \neq \mathbf{z}_1(t^-)$. The difference between $\mathbf{z}_1(t^+)$ and $\mathbf{z}_1(t^-)$ could be large when the power system is subjected to a major failure. Considering these jump changes during the training process can improve the accuracy of the neural model. Intuitively, we should use $\mathbf{z}_1(t^+)$ instead of $\mathbf{z}_1(t^-)$ to predict $\dot{\mathbf{x}}(t)$. However, in most power system simulation tools, jump changes cannot be obtained. An acceptable alternative is to use $\mathbf{z}_1(t+1)$ instead of $\mathbf{z}_1(t)$ to predict $\dot{\mathbf{x}}(t)$ because the variables at the next integration step are a good approximation of the jump changes. Additional equality constraint (24) is added to (6) and constraints (24), (25), and (26) are added to (15) for event handling:

$$\mathbf{z}_{1i}(t^+) = \hat{\mathbf{z}}_{1i}(t+1), t \in T_{event} \quad (24)$$

$$\mathbf{z}_{2i}(t^+) = \hat{\mathbf{z}}_{2i}(t+1), t \in T_{event} \quad (25)$$

$$\mathbf{y}_{1i}(t^+) = \mathbf{g}_\xi(\mathbf{x}_i(t), \mathbf{z}_{2i}(t^+); \xi), t \in T_{event} \quad (26)$$

where T_{event} is the set of time instants when events happen.

E. Integrating Neural Models into Simulator

Intuitively, if the simulator has neural network supportability, i.e., the simulator can load neural networks and perform forward propagation of neural networks, the modified neural ODE module, and the neural DAE module can be easily integrated into the alternating approach of power system transient stability simulations. As for the simultaneous approach, the simulator needs to additionally support backward propagation of neural networks for integrating neural modules. Taking the modified neural ODE module and the Euler's method as an example, as shown in (27), the partial derivatives with respect to the input vector of the neural module are needed, as shown in (28):

$$\mathbf{F}(t) = \mathbf{x}(t) + \Delta t \cdot \mathbf{f}_\theta(\mathbf{x}(t), \mathbf{z}(t); \theta) \quad (27)$$

$$\left[\frac{\partial \mathbf{F}}{\partial \mathbf{x}} \quad \frac{\partial \mathbf{F}}{\partial \mathbf{V}} \right] = \left[\Phi \left(\frac{\partial \mathbf{f}_\theta(\mathbf{x}, \mathbf{z}; \theta)}{\partial \mathbf{x}} \right) \quad \Phi \left(\frac{\partial \mathbf{f}_\theta(\mathbf{x}, \mathbf{z}; \theta)}{\partial \mathbf{V}} \right) \right] \quad (28)$$

where $\Phi(*)$ represents a function of $*$.

F. Possible Applications

In the above subsections, the basic structures and mathematics of the neural modules shown in Fig. 1. (a), (b), and (d) are illustrated. It can be used to build neural dynamic models for almost any dynamic components in power systems. Three possible applications are as follows.

Firstly, they can be used for model calibration. The physical model is "translated" into a neural model. Each parameter is represented by a linear perceptron. The curves of all the variables required by the physical model are needed for the training process. If the L2 norm loss function, it is essentially an integration-based least square method. Meanwhile, some inequality constraints can be added to the loss function to limit

the admissible range of parameters.

Secondly, they can be used for physics-data-integrated dynamic modeling. In practical world, not all the state variables can be easily measured. Therefore, for the state variables that can be easily measured, the derivative functions can be formulated based on physics and neural modules are used for model calibration. The other part of state variables can be modeled using neural networks. Other physical prior knowledge such as network topology can be used to build neural modules by using graph neural networks.

Thirdly, they can be used to build dynamic models based on black-box DLL. Multiple input and output curves are needed for the modeling.

It should be noted that the neural modules can also be used to build equivalent models, e.g., load modeling, wind farm modeling, active distribution network modeling, etc.

G. Autoencoder-based Neural Modules

In Fig. 1. (c) and Fig. 1. (e), the structures of autoencoder-based neural modules are provided. Here, the autoencoder is used to change the dimensionality of the dynamics, as shown in (29).

$$\begin{cases} \mathbf{X}(0) = \text{encoder}(\mathbf{x}(0)) \\ \mathbf{x}(t) = \text{decoder}(\mathbf{X}(t)) \end{cases} \quad (29)$$

where \mathbf{X} is the state variables in hidden space. The encoding process only performs once to transform the initial value into the hidden space. The numerical integration only takes place in the hidden space. The decoding process performs at every integration step including the starting step.

In real-world power systems, dynamic components are not usually completely observable. Only a very limited number of state variables can be measured. In these situations, a dimensionality-raising autoencoder is recommended. On the other hand, in an equivalent modeling situation, there are too many state variables and a low-dimensional manifold usually exists. In this case, a dimensionality reduction autoencoder might be found. The autoencoder-based modules are suggested because they usually outperform the regular ones and the model tuning is easy.

IV. NUMERICAL TESTS

Numerical tests of the proposed modules are carried out. A transient stability simulator that is developed based on our previous studies [34], [35], and [36] is used and a Python API called Py_PSOPS of the simulator is developed and made public [37]. Py_PSOPS is an alternating approach-based electromechanical simulator and is used to generate samples and integrate neural modules. Py_PSOPS can directly load the structure and parameters of neural networks and perform the forward propagation of neural networks.

The test system is the IEEE-39 system. All the components are modeled in detail including the sixth-order generator model, exciters, governors and movers, power system stabilizers (PSS), and induction motor load model. Some simple tests are carried

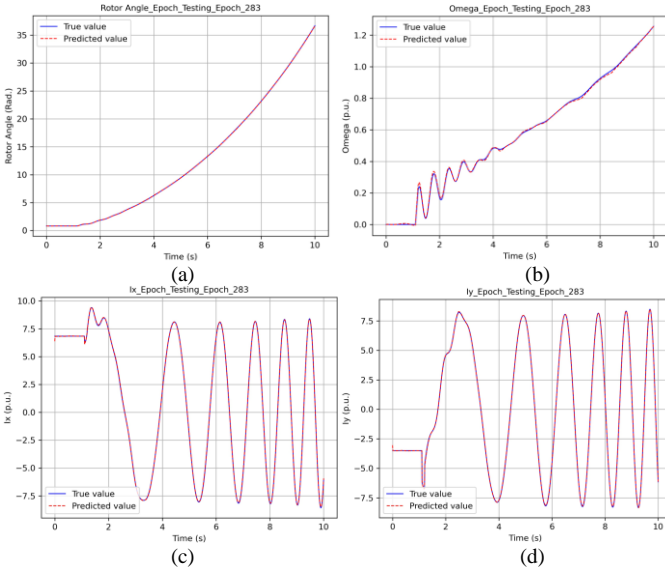


Fig. 2. Test results of the neural DAE module for detailed generator model at BUS-30, including (a) rotor angle, (b) rotation speed, (c) real part of the injection current, and (d) imaginary part of the injection current.

out on the generator connected to BUS-30 to prove the validity and potentiality of the proposed modules. Details of the tests are as follows.

A. Detailed Generator Modeling

As mentioned before, the generator is modeled in detail. A neural DAE module is built to learn the dynamics of the generator. Only the curves of rotor angle and rotation speed are used for the ODE block. The curves of the real part and the imaginary part of the injection current are used for the AE block. Therefore, the variables considered in the neural DAE module are shown in (30).

$$\begin{aligned}
 \mathbf{x}(t) &= \{\delta(t), \omega(t)\} \\
 \mathbf{y}(t) &= \{I_x(t), I_y(t)\} \\
 \mathbf{z}_1(t) &= \{P_g(t), Q_g(t), \mathbf{x}(0), \mathbf{y}(0)\} \\
 \mathbf{z}_2(t) &= \{V_x(t), V_y(t)\}
 \end{aligned} \quad (30)$$

where δ is rotor angle, ω is the rotation speed, I_x and I_y are respectively the real and imaginary parts of the injection current, P_g is the active power, Q_g is the reactive power, and V_x and V_y are respectively the real and imaginary parts of the nodal voltage.

The neural DAE module uses a dimensionality-raising autoencoder. 5000 simulation samples are generated using Py_PSOPS. 4000 samples are used for training and 1000 samples are used for testing. One of the test results is shown in Fig. 2. After training, the neural module can accurately approximate the dynamics of the generator with only the given state variables and operation variables.

B. Generator Model Calibration

Another test is performed for generator model calibration. The generator at BUS-30 is modeled using the classic model. The variables considered in the neural DAE module are shown in (31).

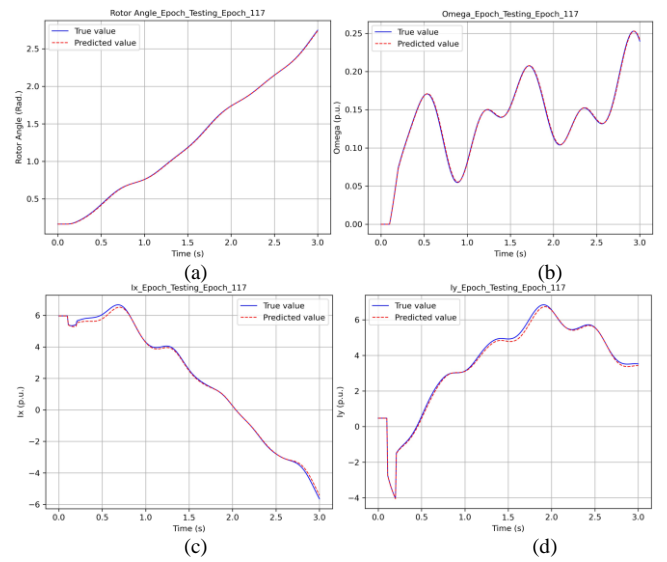


Fig. 3. Test results of the neural DAE module for classic generator model at BUS-30, including (a) rotor angle, (b) rotation speed, (c) real part of the injection current, and (d) imaginary part of the injection current.

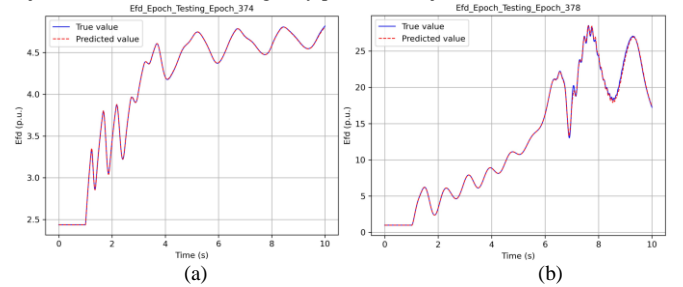


Fig. 4. Test results of the modified neural ODE module for a black-box exciter model at BUS-30 under two different scenarios.

TABLE I
COMPARATIVE RESULTS OF TRAINED PARAMETERS AND GROUND TRUTH

Parameters	Ground Truth	Trained Parameters	Errors
T_j	0.0256364	0.0256043	-0.1252%
x'_d	82.39	82.7518	+0.4391%

$$\begin{aligned}
 \mathbf{x}(t) &= \{\delta(t), \omega(t)\} \\
 \mathbf{y}(t) &= \{I_x(t), I_y(t)\} \\
 \mathbf{z}_1(t) &= \{P_g(t), P_g(0)\} \\
 \mathbf{z}_2(t) &= \{V_x(t), V_y(t)\}
 \end{aligned} \quad (31)$$

The constant time constant T_j and the transient reactance x'_d of the original generator model is replaced by two linear neural cells. 5000 simulation samples are generated, of which 4000 samples are used for training and 1000 are used for testing. One of the test results is shown in Fig. 3. The trained parameters of the neural cells and the comparative results are shown in TABLE I. As can be seen, the learned parameters are accurate enough.

C. Black-box Modeling of an Exciter

The final test is carried out to build a neural dynamic model of a black-box exciter. The variables considered in the modified neural ODE module are shown in (32).

$$\begin{aligned} \mathbf{x}(t) &= \{E_{fd}\} \\ \mathbf{z}_1(t) &= \{V_x(t), V_y(t), \mathbf{x}(0)\} \end{aligned} \quad (32)$$

where E_{fd} is the exciting voltage. Similarly, a dimensionality-raising autoencoder is adopted. The test results are shown in Fig. 4. The neural module works out.

V. CONCLUSION

In this paper, we propose the general frameworks of a modified neural ODE module and a neural DAE module. The mathematics of the backward propagation of these modules is deducted. Besides, the autoencoder-based neural modules are recommended. The numerical tests prove the validity and potentiality of the proposed modules. Future work may focus on designing neural models for equivalent modeling problems, accelerating the training process, and upgrading the performance of the neural modules.

REFERENCES

- [1] N. Hatziargyriou *et al.*, “Definition and Classification of Power System Stability – Revisited amp; Extended,” *IEEE Transactions on Power Systems*, vol. 36, no. 4, pp. 3271–3281, Jul. 2021, doi: 10.1109/TPWRS.2020.3041774.
- [2] J. V. Milanovic, K. Yamashita, S. Martínez Villanueva, S. Ž. Djokic, and L. M. Korunović, “International Industry Practice on Power System Load Modeling,” *IEEE Transactions on Power Systems*, vol. 28, no. 3, pp. 3038–3046, Aug. 2013, doi: 10.1109/TPWRS.2012.2231969.
- [3] P. Kundur, N. J. Balu, and M. G. Lauby, *Power system stability and control*, vol. 7. McGraw-hill New York, 1994.
- [4] A. Honrubia-Escribano, E. Gómez-Lázaro, J. Fortmann, P. Sørensen, and S. Martin-Martinez, “Generic dynamic wind turbine models for power system stability analysis: A comprehensive review,” *Renewable and Sustainable Energy Reviews*, vol. 81, pp. 1939–1952, Jan. 2018, doi: 10.1016/j.rser.2017.06.005.
- [5] S. R. Pendem and S. Mikkili, “Modeling, simulation and performance analysis of solar PV array configurations (Series, Series-Parallel and Honey-Comb) to extract maximum power under Partial Shading Conditions,” *Energy Reports*, vol. 4, pp. 274–287, Nov. 2018, doi: 10.1016/j.egy.2018.03.003.
- [6] R. A. Biroon, P. Pisu, and D. Schoenwald, “Large-Scale Battery Energy Storage System Dynamic Model for Power System Stability Analysis,” in *2020 IEEE Texas Power and Energy Conference (TPEC)*, Feb. 2020, pp. 1–5. doi: 10.1109/TPEC48276.2020.9042536.
- [7] J. K. Noland, E. F. Alves, A. Pardini, and U. Lundin, “Unified Reduced Model for a Dual-Control Scheme of the High-Speed Response Brushless Excitation System of Synchronous Generators,” *IEEE Transactions on Industrial Electronics*, vol. 67, no. 6, pp. 4474–4484, Jun. 2020, doi: 10.1109/TIE.2019.2931270.
- [8] S. Mohajeryami, A. R. Neelakantan, I. N. Moghaddam, and Z. Salami, “Modeling of deadband function of governor model and its effect on frequency Response characteristics,” in *2015 North American Power Symposium (NAPS)*, Oct. 2015, pp. 1–5. doi: 10.1109/NAPS.2015.7335089.
- [9] A. Khodabakhshian, R. Hemmati, and M. Moazzami, “Multi-band power system stabilizer design by using CPCE algorithm for multi-machine power system,” *Electric Power Systems Research*, vol. 101, pp. 36–48, Aug. 2013, doi: 10.1016/j.epsr.2013.03.011.
- [10] A. Arif, Z. Wang, J. Wang, B. Mather, H. Bashualdo, and D. Zhao, “Load Modeling—A Review,” *IEEE Transactions on Smart Grid*, vol. 9, no. 6, pp. 5986–5999, Nov. 2018, doi: 10.1109/TSG.2017.2700436.
- [11] S. Guo, S. Norris, and J. Bialek, “Adaptive Parameter Estimation of Power System Dynamic Model Using Modal Information,” *IEEE Transactions on Power Systems*, vol. 29, no. 6, pp. 2854–2861, Nov. 2014, doi: 10.1109/TPWRS.2014.2316916.
- [12] F. Ding, J. Pan, A. Alsaedi, and T. Hayat, “Gradient-Based Iterative Parameter Estimation Algorithms for Dynamical Systems from Observation Data,” *Mathematics*, vol. 7, no. 5, Art. no. 5, May 2019, doi: 10.3390/math7050428.
- [13] P. Ju, C. Qin, F. Wu, H. Xie, and Y. Ning, “Load modeling for wide area power system,” *International Journal of Electrical Power & Energy Systems*, vol. 33, no. 4, pp. 909–917, May 2011, doi: 10.1016/j.ijepes.2010.12.030.
- [14] B. Yang *et al.*, “Comprehensive overview of meta-heuristic algorithm applications on PV cell parameter identification,” *Energy Conversion and Management*, vol. 208, p. 112595, Mar. 2020, doi: 10.1016/j.enconman.2020.112595.
- [15] R. Huang *et al.*, “Calibrating Parameters of Power System Stability Models Using Advanced Ensemble Kalman Filter,” *IEEE Transactions on Power Systems*, vol. 33, no. 3, pp. 2895–2905, May 2018, doi: 10.1109/TPWRS.2017.2760163.
- [16] R. Fan, R. Huang, and R. Diao, “Gaussian Mixture Model-Based Ensemble Kalman Filter for Machine Parameter Calibration,” *IEEE Transactions on Energy Conversion*, vol. 33, no. 3, pp. 1597–1599, Sep. 2018, doi: 10.1109/TEC.2018.2849856.
- [17] S. R. Khazeiynasab and J. Qi, “Generator Parameter Calibration by Adaptive Approximate Bayesian Computation With Sequential Monte Carlo Sampler,” *IEEE Transactions on Smart Grid*, vol. 12, no. 5, pp. 4327–4338, Sep. 2021, doi: 10.1109/TSG.2021.3077734.
- [18] R. Nagi, X. Huan, and C. Chen, “Bayesian Inference of Parameters in Power System Dynamic Models Using Trajectory Sensitivities,” *IEEE Transactions on Power Systems*, pp. 1–1, 2021, doi: 10.1109/TPWRS.2021.3104536.
- [19] S. Wang, R. Diao, C. Xu, D. Shi, and Z. Wang, “On Multi-Event Co-Calibration of Dynamic Model Parameters Using Soft Actor-Critic,” *IEEE Transactions on Power Systems*, vol. 36, no. 1, pp. 521–524, Jan. 2021, doi: 10.1109/TPWRS.2020.3030164.
- [20] S. rashid R. Khazeiynasab, J. Zhao, I. Batarseh, and B. Tan, “Power Plant Model Parameter Calibration Using Conditional Variational Autoencoder,” *IEEE Transactions on Power Systems*, pp. 1–1, 2021, doi: 10.1109/TPWRS.2021.3107515.
- [21] B. Lusch, J. N. Kutz, and S. L. Brunton, “Deep learning for universal linear embeddings of nonlinear dynamics,” *Nature Communications*, vol. 9, no. 1, Art. no. 1, Nov. 2018, doi: 10.1038/s41467-018-07210-0.
- [22] R. T. Q. Chen, Y. Rubanova, J. Bettencourt, and D. K. Duvenaud, “Neural Ordinary Differential Equations,” *Advances in Neural Information Processing Systems*, vol. 31, pp. 6571–6583, 2018.
- [23] P. Zhang and Y. Zhou, “Neuro-Reachability of Networked Microgrids,” *IEEE Transactions on Power Systems*, pp. 1–1, 2021, doi: 10.1109/TPWRS.2021.3085706.
- [24] Z. Li *et al.*, “Fourier Neural Operator for Parametric Partial Differential Equations,” *arXiv:2010.08895 [cs, math]*, Oct. 2020, Accessed: Nov. 05, 2020. [Online]. Available: <http://arxiv.org/abs/2010.08895>
- [25] M. Mattheakis, D. Sondak, A. S. Dogra, and P. Protopapas, “Hamiltonian Neural Networks for solving differential equations,” *arXiv:2001.11107 [physics]*, Feb. 2020, Accessed: Aug. 14, 2021. [Online]. Available: <http://arxiv.org/abs/2001.11107>
- [26] M. Cranmer, S. Greydanus, S. Hoyer, P. Battaglia, D. Spergel, and S. Ho, “Lagrangian Neural Networks,” *arXiv:2003.04630 [physics, stat]*, Jul. 2020, Accessed: Aug. 14, 2021. [Online]. Available: <http://arxiv.org/abs/2003.04630>
- [27] H. W. Dommel and N. Sato, “Fast Transient Stability Solutions,” *IEEE Transactions on Power Apparatus and Systems*, vol. PAS-91, no. 4, pp. 1643–1650, Jul. 1972, doi: 10.1109/TPAS.1972.293341.
- [28] L. S. Pontryagin, *Mathematical Theory of Optimal Processes*, 1st ed. Routledge, 1962. doi: 10.1201/9780203749319.
- [29] M. Benning, E. Celledoni, M. J. Ehrhardt, B. Owren, and C.-B. Schönlieb, “Deep learning as optimal control problems: models and numerical methods,” *arXiv:1904.05657 [cs, math]*, Sep. 2019, Accessed: Nov. 13, 2020. [Online]. Available: <http://arxiv.org/abs/1904.05657>
- [30] D. P. Kingma and J. Ba, “Adam: A Method for Stochastic Optimization,” *arXiv:1412.6980 [cs]*, Jan. 2017, Accessed: Dec. 09, 2020. [Online]. Available: <http://arxiv.org/abs/1412.6980>
- [31] “PyTorch.” <https://pytorch.org/>
- [32] J. Zhuang, N. Dvornek, X. Li, S. Tatikonda, X. Papademetris, and J. Duncan, “Adaptive Checkpoint Adjoint Method for Gradient Estimation in Neural ODE,” in *International Conference on Machine Learning*, Nov. 2020, pp. 11639–11649. Accessed: Sep. 05, 2021. [Online]. Available: <https://proceedings.mlr.press/v119/zhuang20a.html>
- [33] J. Zhuang, N. C. Dvornek, S. Tatikonda, and J. s Duncan, “MALI: A memory efficient and reverse accurate integrator for Neural ODEs,” presented at the International Conference on Learning Representations, Sep. 2020. Accessed: Jul. 25, 2021. [Online]. Available: https://openreview.net/forum?id=blfSjHeFM_e

- [34] T. Xiao, J. Wang, Y. Gao, and D. Gan, "Improved Sparsity Techniques for Solving Network Equations in Transient Stability Simulations," *IEEE Trans. Power Syst.*, vol. 33, no. 5, pp. 4878–4888, Sep. 2018, doi: 10.1109/TPWRS.2018.2803200.
- [35] T. Xiao, W. Tong, and J. Wang, "A New Fully Parallel BBDF Method in Transient Stability Simulations," *IEEE Trans. Power Syst.*, vol. 35, no. 1, pp. 304–314, Jan. 2020, doi: 10.1109/TPWRS.2019.2933637.
- [36] T. Xiao, W. Tong, and J. Wang, "Study on Reducing the Parallel Overhead of the BBDF Method for Power System Transient Stability Simulations," *IEEE Trans. Power Syst.*, vol. 35, no. 1, pp. 539–550, Jan. 2020, doi: 10.1109/TPWRS.2019.2929775.
- [37] T. Xiao, Y. Chen, J. Wang, S. Huang, W. Tong, and T. He, "Exploration of AI-Oriented Power System Transient Stability Simulations," *arXiv:2110.00931 [cs, eess]*, Oct. 2021, Accessed: Oct. 24, 2021. [Online]. Available: <http://arxiv.org/abs/2110.00931>